PHOTOLUMINESCENCE LIFETIME SPECTROSCOPY - SURFACE RECOMBINATION ANALYSIS

T. Roth[1,*], M. Rüdiger[1], P. Rosenits[1], S. Diez[1,2], T. Trupke[3], R.A. Bardos[3], S.W. Glunz[1]

[1]) Fraunhofer Institute for Solar Energy Systems ISE
Heidenhofstrasse 2, 79110 Freiburg, Germany

[*]) Phone: +49 761 4588 5610, Fax: +49 761 4588 9250, Email: thomas.roth@ise.fraunhofer.de

[2]) now with: Q-Cells AG, Guardianstrasse 16, 06766 Thalheim, Germany

[3]) Centre of Excellence for Advanced Silicon Photovoltaics and Photonics
University of New South Wales, Sydney, 2052, Australia

ABSTRACT: The recently introduced quasi-steady-state photoluminescence technique (QSS-PL) for determining the injection-dependent carrier lifetime in silicon samples was shown to be a good complement of the well established quasi-steady-state photoconductance technique (QSS-PC) especially in the low injection regime, where the QSS-PC technique is prone to measurement artefacts due to trapping or depletion region modulation. The ability to measure the real recombination lifetime at low injection densities makes the QSS-PL an ideal tool for the analysis and subsequent modelling of the surface recombination velocity. In this contribution a thickness and resistivity varied sample set of SiO_2 passivated silicon samples is used to investigate the injection-dependent surface recombination velocity. Modelling of these experimental data with a recent model yields the relevant surface parameters for the investigated passivation. In addition, corona charging is used for further reduction of the surface recombination velocity in order to gain additional knowledge of the sample surface.

Keywords: Photoluminescence, Surface Recombination, Silicon

1 INTRODUCTION

Different experimental techniques are used at Fraunhofer ISE for measurements of the injection-dependent carrier lifetime of silicon samples. Two examples of commonly used measurement approaches are the microwave-detected photoconductance decay technique (µW-PCD) [1] and the quasi-steady-state photoconductance technique (QSS-PC) using the WCT-100 / 120 [2].

Recently a new approach to measure the injection-dependent lifetime was introduced using quasi-steady-state photoluminescence lifetime measurements (QSS-PL) [3]. This measurement technique is affected neither by excess carriers accumulated in space charge regions [4], nor by trapping [5], which is particularly important for measurements of the low injection limit of the effective lifetime.

Knowledge of the surface recombination parameters and the underlying physical model is of both theoretical and technological interest.

In this contribution it will be shown how QSS-PL can be used to investigate the surface recombination velocity of SiO_2 passivated silicon samples down to an injection range of $1x10^{10}$ cm^{-3}, which was not easily possible so far. A set of floatzone (FZ) silicon samples with variable thickness (ranging from 38 µm to 189 µm) and resistivity (0.25, 1, 8, and 100 Ω cm) was used. Subsequent modelling leads to a set of surface parameters for this kind of passivation.

In addition it will be shown how corona charging influences the surface recombination velocity of the SiO_2 passivated samples.

2 SAMPLE PREPARATION

Float-zone silicon wafers with <100> surface orientation were used in this study. Samples of four different resistivities (0.25, 1, 8, 100 Ω cm, all boron-doped p-type) were mechanically thinned using a grinder [6]. This resulted in a thickness variation from 38 µm to 189 µm (for details see Tab. 1). The thinning was followed by a short KOH etch and a RCA clean, before a thermal oxide (105 nm) was grown. The last step was a forming gas anneal (425°C, 60 min).

Tab. 1: Thicknesses after grinding and KOH etch of the various samples used in this study.

ρ (Ωcm)	*Thickness* (µm)							
0.25	39	45	52	62	77	99	127	182
1	52	58	69	83	134	190		
8	47	64	134					
100	38	47	64	135	189			

3 MEASUREMENT SETUP

The schematic of the photoluminescence lifetime measurement setup is shown in Fig. 1.

The sample is illuminated on the front surface with a LED light source (λ = 810 nm). Radiative recombination of photogenerated carriers within the sample results in the emission of photoluminescence (PL), which is detected by a photodetector located on the rear of the sample. Similar to QSS-PC the generation rate in QSS-PL measurements is determined from the incident light intensity, which is monitored separately.

The detected PL intensity is proportional to

$$I_{PL} = A_i\, B(T,\Delta n)\, n\, p = A_i\, B(T,\Delta n)\left(N_{A/D} + \Delta n\right)\Delta n \quad , \tag{1}$$

where A_i is a calibration constant, B the coefficient for radiative recombination, and n/p are the electron and hole carrier densities, respectively. Solving this equation for the

average excess carrier concentration Δn and using the separately monitored generation rate $G(t)$, the injection-dependent carrier lifetime can be determined [7]:

$$\tau_{eff}(\Delta n) = \frac{\Delta n(t)}{G(t) - \frac{d\Delta n(t)}{dt}} \quad . \qquad (2)$$

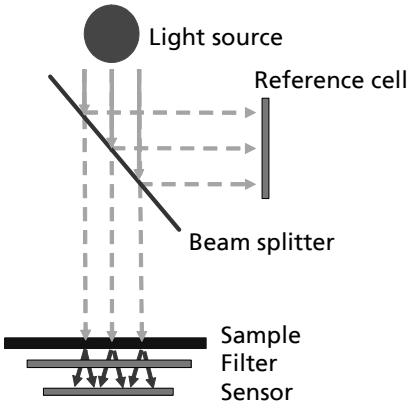

Fig. 1: Schematic of the photoluminescence (PL) measurement setup. The sample is illuminated via a LED light source. The emitted PL light emitted from the rear surface is detected by an external sensor. The generation rate is monitored using a calibrated reference cell.

4 MEASUREMENT RESULTS

4.1 Experimental data

Injection level dependent effective lifetime values were measured by means of QSS-PC and QSS-PL. The two systems are somewhat complementary as they yield the lifetime reliably in different injection ranges. The current QSS-PL setup at Fraunhofer ISE covers the injection range from $1x10^{9}$ cm^{-3} to $1x10^{14}$ cm^{-3} (for wafers with typical lifetimes of a few tens of microseconds). The flash used in QSS-PC allows much higher injection levels to be measured. QSS-PC covers the injection range $\Delta n > 1x10^{13}$ cm^{-3}. In this study QSS-PL measurements were calibrated against QSS-PC measurements for the 0.25 and 1 Ω cm samples. For the 8 and 100 Ω cm samples this was not possible since the QSS-PC measurements were affected by measurement artefacts, whose origin is unknown so far. A self consistent calibration method [8] was used for these samples.

As an example, the resulting lifetime curves of the 1 Ω cm samples are shown in Fig. 2. All curves have been corrected for Auger recombination in the high injection part [9].

In order to extract the surface recombination velocity S from the measured effective lifetime data, the following equation has been used, which holds for adequate small values of S [10]:

$$\frac{1}{\tau_{eff}} = \frac{1}{\tau_{bulk}} + \frac{2S}{W} \quad , \qquad (3)$$

where τ_{bulk} denotes the bulk lifetime and W the sample thickness. Assuming a FZ-Si bulk lifetime in the order of milliseconds, the bulk term has been disregarded in order to simplify the analysis. In addition, measurement data, where the above approximations of equation (3) lead to errors larger than 20% in the calculated S have been rejected. This was necessary for the low injection data of the 0.25 Ω cm sample for the sake of easy evaluation.

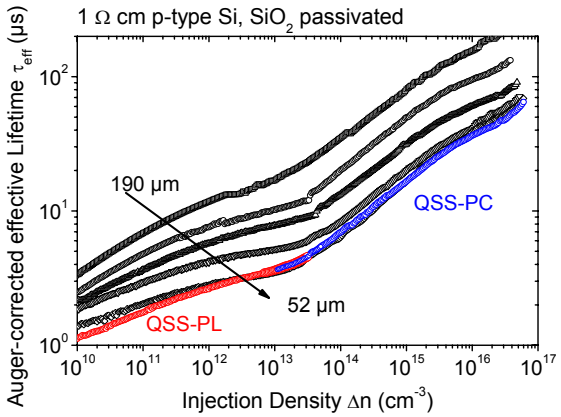

Fig. 2: Injection-dependent effective lifetimes for the 1 Ω cm samples. Lifetimes were measured with QSS-PL and QSS-PC. All curves are corrected for Auger recombination.

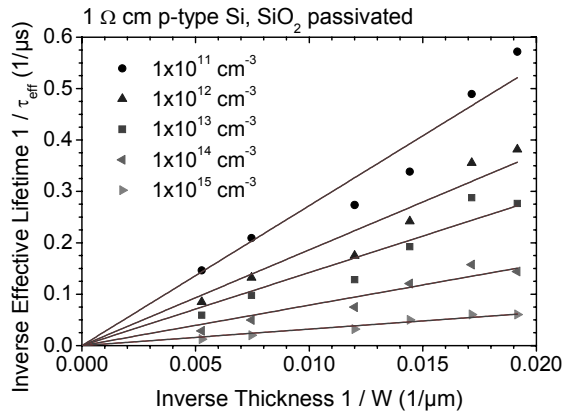

Fig. 3: Inverse effective lifetimes vs. inverse thickness for different injection densities of the 1 Ω cm samples. From the slope of each line of best fit, the surface recombination velocity can be calculated.

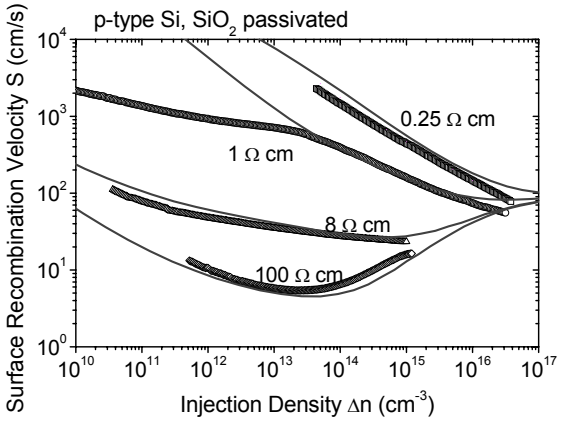

Fig. 4: Experimentally extracted data for the injection-dependent surface recombination velocity. The grey solid lines show the model data.

From the slope of a $1/\tau_{eff}$ vs. $1/W$ plot (see Fig. 3), the injection-dependent S has been extracted for the four different sample sets (see Fig. 4). As expected, the higher the base resistivity of the samples, the better the passivation quality. The origin of the kink in the 1 Ω cm curve which we reproducibly observed in QSS-PL lifetime curves measured on various samples in unclear at this stage.

4.2 Modelling

For the modelling of the experimental data of the injection-dependent surface recombination velocity, a model has been used, which includes spatial fluctuations of the surface potential due to an inhomogeneous charge distribution in the oxide. In addition the model accounts for shunt currents through the space-charge region, which are described via a shunt resistor R_P and recombination within the space-charge region J_{02}. For the energy dependence of the electron and hole capture cross sections and the energy distribution of the interface trap density, measured values from [9] have been used, where also some more details about the model can be found.

All four curves in Fig. 4 have been modelled using the same parameter set, with exception of the doping concentration, which is listed in Tab. 2.

As can be seen, the model describes the experimental data quite well, except for the low injection part of the 1 Ω cm sample. The reason for this discrepancy is unclear so far but appears to be related to the kink observed in Fig. 2.

Tab. 2: Parameters used for the modelling of the measured surface recombination velocity. The parameters for the capture cross sections and the energy distribution can be found in [9].

Parameter	Explanation	Value
$D_{it,midgap}$	Interface density at midgap	$1x10^{11}$ eV^{-1} cm^{-2}
Q_f	Fixed oxide charge	$1.9x10^{11}$ cm^{-3}
σ_g	Width of Gaussian distribution of surface potential	2.0 kT/q
R_p	Shunt resistance	$1x10^{7}$ Ω cm^2
J_{02}	Diode saturation current	$5x10^{-10}$ A cm^{-2}

5 CORONA CHARGING

The influence of the surface on the effective lifetime measurements can also be demonstrated by applying a corona charge to the oxide.

5.1 Deposition of corona charges

The setup for the deposition of corona charges is shown in Fig. 5. The charges are generated by applying a voltage of 10 kV to a set of four tungsten needles. The high electric field in the range of the tips ionises air particles and molecules. The charges are attracted by the grounded sample. Variation of the gate potential allows the amount of charges deposited on the sample to be controlled easily. In addition, the lateral distribution of charges on the sample is much more homogeneous. The deposited corona charge is measured using a Kelvin probe [11]. More details about the setup can be found in [9].

5.2 Results

Measurements with strong positive (+18V) and strong negative (-18V) corona charges have been performed on some of the 1 Ω cm samples. Using the same calculations as in section 4.1, the surface recombination velocities S have been calculated, as shown in Fig. 6.

The corona charge has different impact at different injection densities. Compared to the neutral state, the deposition of positive charge on the oxide lowers S at an injection density higher than $1x10^{12}$ cm^{-3}, while below this injection density S is increased. The impact of a negative corona charge is different: below an injection density of about $1x10^{15}$ cm^{-3} S is decreased and very constant over the whole injection range. A small increase in S can be observed at an injection density above $2x10^{15}$ cm^{-3}. It was not possible to model these experimental data with the model presented before, implying that there are additional physical aspects influencing S, which are not accounted for in the model. This will be covered in further studies.

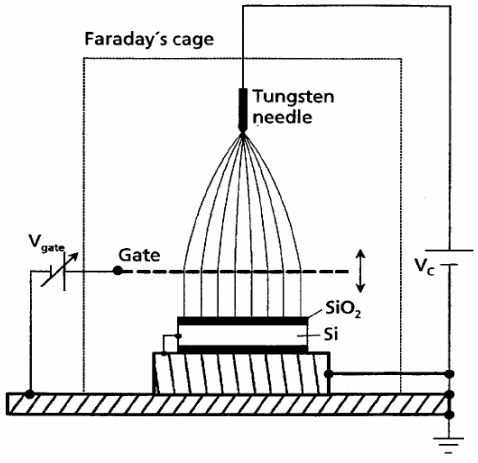

Fig. 5: Schematic of the corona charging setup.

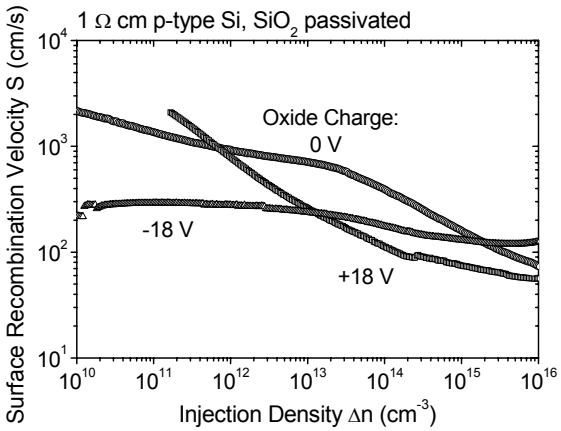

Fig. 6: Measured surface recombination velocities for the 1 Ω cm samples with different corona charges.

6 DISCUSSION

6.1 Application to other passivation techniques

Fig. 7 shows the measured effective lifetimes and extracted surface recombination velocities for a set of 1 Ω cm p-type silicon samples, which were passivated using plasma enhanced chemical vapour deposition (PECVD) SiN_x with a subsequent sintering step. The fact that no kink is observed in the surface recombination velocity shows that the effect observed in the oxide passivated samples (Fig.2) is real and not a measurement artefact.

The graph shows a slightly different curve shape compared to the SiO_2 samples due to the different underlying physical principle of the passivation.

As has been done for the SiO_2 samples, different resistivities of the SiN_x samples will be investigated in the future, in order to model these data, so that the parameters are accessible.

This example shows, that the surface recombination analysis using lifetime spectroscopic devices is not limited to a certain kind of surface passivation, but also allowing other kinds of passivation techniques like silicon carbide (SiC) or amorphous silicon (a-Si) to be investigated.

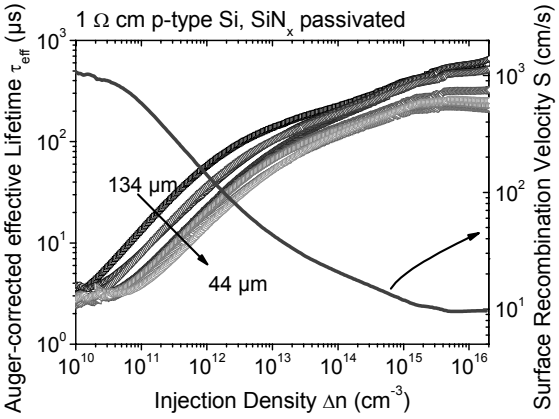

Fig. 7: Effective lifetimes and extracted surface recombination velocity for a set of 1 Ω cm p-type Si samples, passivated with SiN_x (PECVD).

6.2 Impact on defect spectroscopy

The QSS-PL was found to be an ideal extension for the well established QSS-PC in the field of defect spectroscopy, since it is affected neither by trapping nor by depletion region modulation measurement artefacts. In advanced defect spectroscopy methods the quantity that is of interest is the bulk lifetime. As the measurements presented here have shown, care has to be taken when interpreting the measured effective lifetime data. In order to extract the Shockley-Read-Hall bulk lifetime, the data have to be corrected for surface recombination. In contrast to the intrinsic Auger recombination, in which case the lifetime data can be easily corrected for, the surface recombination depends to a certain extent on the used process parameters, making a correction difficult.

7 SUMMARY

Knowledge of the surface recombination parameters and the underlying physical model is of both theoretical and technological interest.

In order to obtain the injection-dependent surface recombination velocity, the QSS-PL method has been used to measure the effective carrier lifetime at low injection, whereas the QSS-PC method has been used to access the lifetime at higher injection levels.

As has been presented in this paper, QSS-PL makes the very low injection range easily accessible for lifetime measurements, hence allowing the surface recombination velocity to be analysed. The use of sample sets with variable thickness resulted in very reliable data for the extracted surface recombination velocity for different resistivities.

For different base resistivities it was possible to model the injection-dependent surface recombination velocities for SiO_2 passivated Si samples, using a recent model. Nevertheless, as the measurements of corona charged samples showed, additional physical effects are influencing the surface recombination velocity, which have to be investigated in the future. The measurement data, which have been gained in an injection range from $1x10^{10}$ cm^{-3} to $2x10^{16}$ cm^{-3} are a solid basis for further investigations and show the possibilities of this method for accessing the surface recombination velocity in a wide injection range.

Summarising, the QSS-PL together with the QSS-PC is an ideal tool for accessing the surface recombination velocity of various passivation techniques, such as SiO_2, SiN_x, a-Si and SiC. The corona charging is an additional instrument to extend the physical understanding of surface recombination by varying an additional parameter.

Based on the experimental data for the surface recombination velocity, nearly all measured lifetime samples are affected by surface recombination at low injection densities, which has to be considered when using such lifetime measurements for defect spectroscopy.

8 ACKNOWLEDGEMENTS

The authors would like to thank H. Kampwerth for sample preparation and J. Holtkamp for measurements.

Thomas Roth gratefully acknowledges a scholarship of the German Federal Environmental Foundation (Deutsche Bundesstiftung Umwelt). Marc Rüdiger gratefully acknowledges a scholarship of the Evangelisches Studienwerk e.V. Villigst.

9 REFERENCES

[1] S.W. Glunz, J. Schumacher, W. Warta, J. Knobloch and W. Wettling, Progress in Photovoltaics: Research and Applications **4** (1996) 415.

[2] R.A. Sinton, A. Cuevas and M. Stuckings, Proceedings of the 25th IEEE Photovoltaic Specialists Conference, Washington DC, USA (1996) 457.

[3] T. Trupke, R.A. Bardos, F. Hudert, P. Würfel, J. Zhao, A. Wang and M.A. Green, Proceedings of the 19th European Photovoltaic Solar Energy Conference, Paris, France (2004) 758.

[4] T. Trupke and R.A. Bardos, Proceedings of the 31st IEEE Photovoltaic Specialists Conference, Orlando, Florida, USA (2005) 903.

[5] R.A. Bardos, T. Trupke, M.C. Schubert and T. Roth, Applied Physics Letters **88** (2006) 053504.

[6] H. Kampwerth, S. Rein and S.W. Glunz, Proceedings of the 3rd World Conference on Photovoltaic Energy Conversion, Osaka, Japan (2003) 1073.

[7] H. Nagel, C. Berge and A.G. Aberle, Journal of Applied Physics **86** (1999) 6218.

[8] T. Trupke, R.A. Bardos and M.D. Abbott, Applied Physics Letters **87** (2005) 184102.

[9] S.W. Glunz, D. Biro, S. Rein and W. Warta, Journal of Applied Physics **86** (1999) 683.

[10] A.B. Sproul, Journal of Applied Physics **76** (1994) 2851.

[11] L. Kelvin, Phil. Mag. **46** (1898) 82.